

---

# Associations between iron and mean kurtosis in iron-rich grey matter nuclei in aging

Jason Langley<sup>1\*</sup>, Kitzia Solis<sup>2</sup>, Vala Masjedizadeh<sup>3</sup>, Ilana Bennett<sup>2</sup>, and Xiaoping P. Hu<sup>1,3</sup>

<sup>1</sup> Center for Advanced Neuroimaging, University of California Riverside, Riverside, CA, USA

<sup>2</sup> Department of Psychology, University of California Riverside, Riverside, CA, USA

<sup>3</sup> Department of Bioengineering, University of California Riverside, Riverside, CA, USA

+jason 'dot' langley 'at' ucr.edu

## Abstract

Mean kurtosis in iron-rich grey matter has values similar to that seen in white matter. We suspect these elevated values may be related to iron. Multi-shell diffusion and multi-echo gradient echo acquisitions were used to derive mean kurtosis and  $R_2^*$ , respectively. Mean kurtosis and  $R_2^*$  were measured in subcortical grey matter nuclei and white matter tracts in 93 older adults and 62 younger adults. Grey matter regions exhibited higher mean kurtosis and  $R_2^*$  in the older adult group whereas white matter regions had reduced mean kurtosis in the older adult group. Grey matter mean kurtosis was significantly correlated with  $R_2^*$  iron-rich grey matter nuclei in both groups. Our findings indicate that higher mean kurtosis in iron-rich grey matter structures may be due to either increased tissue complexity or to decreases in signal-to-noise ratios from iron deposition.

Keywords: kurtosis, iron, grey matter, aging

---

## 1. Introduction

Magnetic resonance imaging (MRI) techniques that are sensitive to the diffusion of water have been used to study effects of normal aging<sup>1-3</sup> or disease<sup>4-6</sup> on brain tissue microstructure. Diffusion tensor imaging (DTI) is a commonly used approach that models tissue as a single compartment with the assumption that diffusion is Gaussian. However, the cells, organelles, and cell membranes that comprise tissue can introduce barriers to diffusion and cause it to be a non-Gaussian process. Diffusion kurtosis imaging (DKI) is able to characterize non-Gaussian diffusion by relaxing this assumption<sup>7</sup> and measures the degree to which diffusion differs from a Gaussian process, known as kurtosis. Higher kurtosis values are thought to be indicative of more complex tissue microstructure<sup>8,9</sup>.

Application of DKI to aging has consistently revealed lower kurtosis values in white matter tracts of older adults relative to younger adults<sup>10-15</sup>, consistent with evidence that aging is accompanied by degradation of white matter<sup>16,17</sup>, which would remove barriers to diffusion and manifest as lower MK<sup>8,18</sup>. In contrast, results have been mixed in subcortical grey matter nuclei, with lower kurtosis in older than younger adults in the caudate and thalamus, but higher kurtosis in older than younger adults in the putamen<sup>11,12</sup>.

Higher kurtosis has also been seen in the globus pallidus, putamen, and substantia nigra in participants with neurodegenerative disorders (Parkinson's Disease) relative to age-matched controls<sup>19,20</sup>. Whereas the mechanism for this increase is unknown<sup>19</sup>, its occurrence in grey matter nuclei that accumulate iron throughout the lifespan<sup>21-25</sup> suggests that iron content may affect kurtosis. Iron is known to alter DTI metrics (mean diffusivity, fractional anisotropy) within iron-rich grey matter nuclei in aging and disease<sup>26-28</sup> and has been attributed to an interaction between diffusion encoding gradients and the magnetic fields generated by iron deposits<sup>29,30</sup>. However, the effect of iron on diffusion kurtosis remains unknown.

The purpose of the present study was to test the hypothesis that elevated iron is a mechanism driving elevated kurtosis values in subcortical grey matter. In younger and older adults who underwent DKI, we characterized age group differences in iron and kurtosis in subcortical grey matter structures as well as in white matter tracts and then examined relationships between measures of iron and kurtosis in subcortical grey matter structures. To further test this relationship, we measured kurtosis in an agarose phantom with four levels of iron concentrations.

## 2. Methods

## 2.1 Participants

A cohort consisting of 93 older adults (56 female/37 male; mean age=69.5 years  $\pm$  6.0 years; age range: 60 years–87 years) and 62 younger adults (41 female/21 male; mean age=20.2 years  $\pm$  2.0 years; age range: 18 years–28 years) participated in this study. Each participant gave written informed consent prior to enrolling in the study as approved by the local institutional review board.

## 2.2 Structural acquisition and processing

Images from a T<sub>1</sub>-weighted MP-RAGE sequence (echo time (TE)/repetition time (TR)/inversion time=3.02/2600/800 ms, flip angle=8°, voxel size=0.8×0.8×0.8 mm<sup>3</sup>) were used for registration from subject space to common space. T<sub>1</sub>-weighted images were analyzed with FMRIB Software Library (FSL). A transformation was derived between individual subject space to MNI152 T<sub>1</sub>-weighted space using FMRIB's Linear Image Registration Tool (FLIRT) and FMRIB's Nonlinear Image Registration Tool (FNIRT) in the FSL software package<sup>31,32</sup>.

## 2.3 Diffusion acquisition and processing

Diffusion-weighted data were acquired using a spin-echo EPI with bipolar diffusion encoding gradients with the following parameters: TE/TR = 102/3500 ms, FOV = 212×182 mm, voxel size = 1.7×1.7×1.7 mm, 64 axial slices, six  $b=0$  images, and multiband acceleration factor = 4. Diffusion-weighting was applied in 64 directions with two  $b$ -values ( $b=1500$  s/mm<sup>2</sup> and  $b=3000$  s/mm<sup>2</sup>). Six  $b=0$  images with reversed phase-encoding were acquired to correct for susceptibility distortions.

Diffusion data were denoised in *mrtrix*<sup>33</sup>, then corrected for motion, eddy current and susceptibility distortions using *eddy* in FSL<sup>34</sup>. Next, skull stripping of the T<sub>1</sub>-weighted image and susceptibility corrected  $b=0$  image was performed using the brain extraction tool in the FSL software package<sup>35</sup>. Mean kurtosis (MK) was estimated in *DIPY*<sup>36</sup>.

## 2.4 Iron acquisition and processing

Multi-echo data were collected with a 6-echo 3D gradient recalled echo sequence: TE<sub>1</sub>/ΔTE/TR =4/6/40 ms, FOV=192×224 mm<sup>2</sup>, matrix size=192×224×96, and slice thickness=1.7 mm. R<sub>2</sub><sup>\*</sup> was calculated from the magnitude data assuming a mono-exponential decay.

## 2.5 Regions of interest

Globus pallidus, putamen, caudate nucleus, thalamus, and hippocampus regions of interest (ROIs) were defined using the Harvard-Oxford subcortical atlas and the dentate nucleus was defined using a previously published atlas<sup>37</sup>. MK and mean R<sub>2</sub><sup>\*</sup> were measured in each grey matter ROI. White matter ROIs for the superior longitudinal fasciculus, forceps major, and forceps minor were defined using the Johns-Hopkins white matter atlas and mean MK was

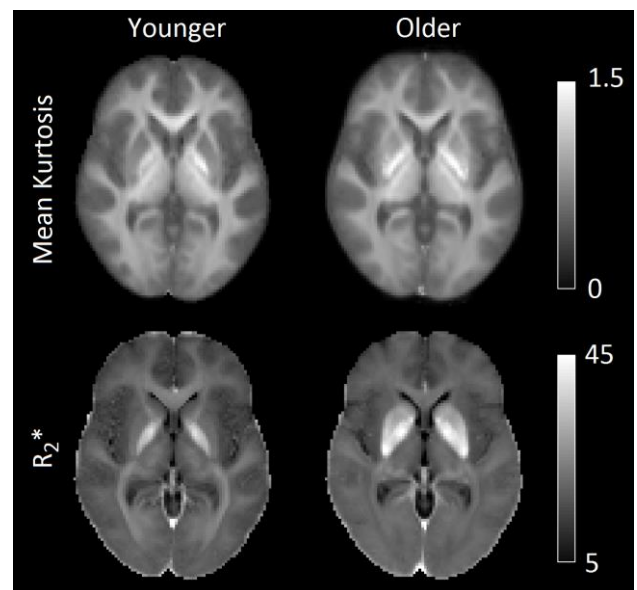


**Figure 1.** Group average images for mean kurtosis (top row) and R<sub>2</sub><sup>\*</sup> (bottom row) in younger (left column) and older (right column) participants. These images were created by transforming each participant's mean kurtosis and R<sub>2</sub><sup>\*</sup> map to Montreal Neurological Institute (MNI) common space and averaging within each group.

measured in each ROI. For each ROI, voxels with MK values that were negative or greater than 4 were excluded.

## 2.6 Phantom Experiment

An agar phantom (2.5% agarose) was constructed with 4 vials of ferric citrate embedded in the phantom (2.5% agarose; ferric citrate concentrations: 0.06 mMol, 0.09 mMol, 0.12 mMol, 0.15 mMol). The phantom was scanned with a diffusion-weighted acquisition (TE/TR=70/4000 ms; voxel size=1.4 mm isotropic, 30 diffusion directions with  $b=1000$  s/mm<sup>2</sup> and  $b=2000$  s/mm<sup>2</sup>, 3  $b=0$  images were acquired, 15 averages). A second diffusion acquisition with identical parameters but with reverse phase encoding was acquired to correct for susceptibility distortions. Data were processed as in the human scans. Data were denoised in *mrtrix*<sup>33</sup>, then corrected for eddy current and susceptibility distortions using *eddy* in FSL. Mean kurtosis (MK) was estimated in *DIPY*<sup>36</sup>. ROIs were placed in each vial and a control ROI was placed in a region with no iron at the center of the phantom.

## 2.5 Statistical Analysis

All statistical analyses were performed using IBM SPSS Statistics software version 24 (IBM Corporation, Somers, NY, USA) and results are reported as mean  $\pm$  standard deviation. A  $P$  value less than 0.05 was considered significant for all statistical tests. Age group MK and R<sub>2</sub><sup>\*</sup> comparisons between the young and older cohort were made using a 2 Group (younger, older)  $\times$  9 (subcortical grey matter and white matter) Region analysis of variance (ANOVA) for

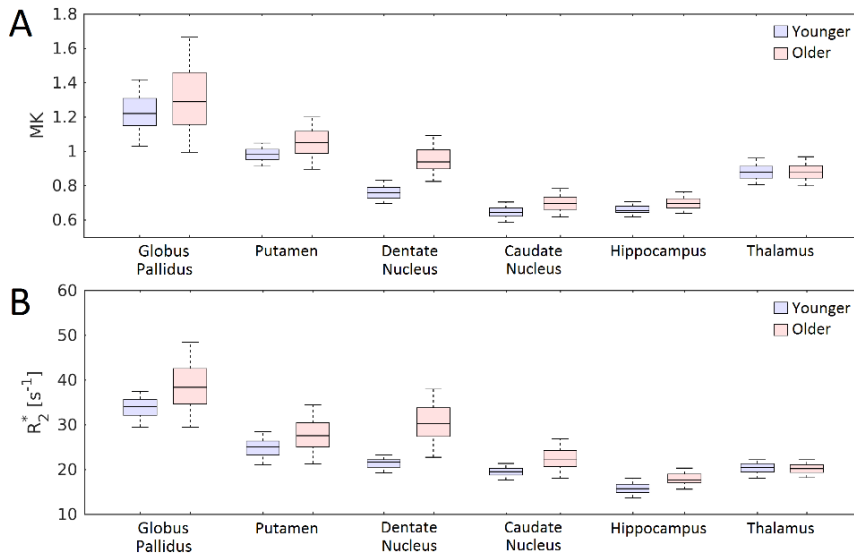


**Figure 2.** Group comparisons of mean kurtosis (MK; shown in A) and  $R_2^*$  (shown in B) for all grey matter ROIs considered in this analysis. Significant increases in MK and  $R_2^*$  were observed in the pallidum, putamen, dentate nucleus, caudate nucleus, and hippocampus of the older adult group relative to the younger adult group. No difference in MK or  $R_2^*$  was seen in the thalamus.

MK comparison and separate 2 Group (younger, older)  $\times$  6 Region (subcortical grey matter) ANOVA for  $R_2^*$ . Significant interactions were followed with *post hoc* between-group two-tailed *t*-tests for each region.

Within older adults, relationships between age and both MK and iron ( $R_2^*$ ) measures were assessed with separate Pearson correlations. These relationships were not assessed in younger adults due to their restricted age range.

To assess the relationship between iron and MK in subcortical grey matter, Pearson correlations between iron measures ( $R_2^*$ ) and MK in grey matter ROIs were performed separately in each age group.

In the phantom experiment, the effect of iron concentration on MK was tested with a 5 Concentration (0, 0.06, 0.09, 0.12, 0.15) one-way ANOVA. If the interaction was significant, *post hoc* comparisons between MK values in each vial were performed using respective two-tailed *t*-tests.

### 3. Results

#### 3.1 Age group differences in mean kurtosis

Maps of MK in each age group are shown in **Figure 1**. Significant main effects of Group ( $P < 10^{-3}$ ;  $F = 106.110$ ) and region ( $P < 10^{-3}$ ;  $F = 683.775$ ) were seen in the 2 Group (younger, older)  $\times$  9 (subcortical grey matter and white matter) Region ANOVA. A significant interaction was observed between Group and Region ( $P < 10^{-3}$ ;  $F = 23.469$ ). *Post hoc* *t*-tests revealed that the older adult group had higher MK than the younger group in the putamen ( $P < 10^{-3}$ ), globus pallidus ( $P = 0.001$ ), caudate nucleus ( $P < 10^{-3}$ ), dentate nucleus ( $P < 10^{-3}$ ), and hippocampus ( $P = 0.048$ ), but not in the thalamus ( $P = 0.446$ ). In white matter ROIs, the older adult group had lower MK than the younger group in the superior longitudinal fasciculus ( $P < 10^{-3}$ ), forceps major ( $P = 0.029$ ), and forceps minor ( $P < 10^{-3}$ ). These comparisons are shown in

**Figures 2 and 3** and mean values for each group are summarized in **Table 1**.

#### 3.2 Effects of age on mean kurtosis in older adults

In subcortical grey matter structures of the older adult group, older age was correlated with lower MK in the caudate nucleus ( $r = -0.225$ ;  $P = 0.030$ ), thalamus ( $r = -0.256$ ;  $P = 0.013$ ), and hippocampus ( $r = -0.215$ ;  $P = 0.038$ ). No significant correlations were observed in the globus pallidus ( $r = -0.199$ ;  $P = 0.055$ ), putamen ( $r = 0.057$ ;  $P = 0.591$ ), or dentate nucleus ( $r = -0.065$ ;  $P = 0.539$ ). In white matter tracts of the older adult group, older age was significantly associated with lower MK in the superior longitudinal fasciculus ( $r = -0.414$ ;  $P < 10^{-3}$ ), forceps major ( $r = -0.346$ ;  $P < 10^{-3}$ ), and forceps minor ( $r = -0.344$ ;  $P < 10^{-3}$ ).

#### 3.3 Age group differences in $R_2^*$

Maps of mean  $R_2^*$  in each age group are shown in **Figure 1**. Significant main effects of Group ( $P < 10^{-3}$ ;  $F = 218.335$ ) and region ( $P < 10^{-3}$ ;  $F = 498.607$ ) were seen in the

**Table 1.** Age group differences in mean kurtosis

	Younger	Older	<i>t</i>
Putamen	0.75 $\pm$ 0.05	0.95 $\pm$ 0.11	<b>176.86</b>
Globus Pallidus	1.23 $\pm$ 0.12	1.33 $\pm$ 0.23	<b>10.55</b>
Caudate Nucleus	0.65 $\pm$ 0.04	0.70 $\pm$ 0.59	<b>44.43</b>
Dentate Nucleus	0.99 $\pm$ 0.06	1.06 $\pm$ 0.10	<b>22.29</b>
Thalamus	0.88 $\pm$ 0.05	0.89 $\pm$ 0.06	0.585
Hippocampus	0.66 $\pm$ 0.03	0.70 $\pm$ 0.04	<b>38.52</b>
Sup. Long. Fasc.	0.99 $\pm$ 0.03	0.96 $\pm$ 0.05	<b>18.60</b>
Forceps Major	0.77 $\pm$ 0.03	0.75 $\pm$ 0.04	<b>4.88</b>
Forceps Minor	0.89 $\pm$ 0.04	0.86 $\pm$ 0.06	<b>13.78</b>

*Notes.* Mean kurtosis values in subcortical grey matter regions of interest and white matter tracts. Data is presented as mean  $\pm$  standard deviation. *Post hoc t*-tests were used for group comparisons of MK in each ROI from which the *t*-statistics are shown.

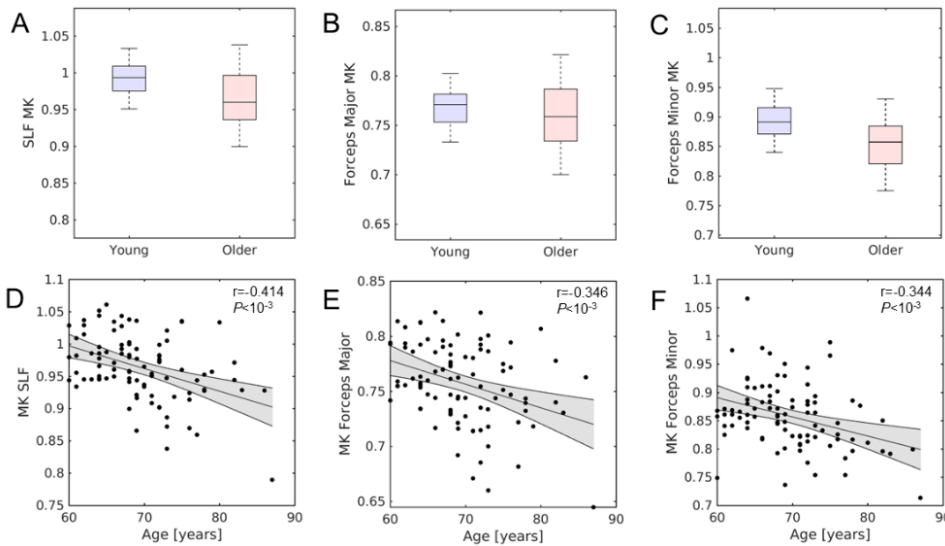


**Figure 3.** Group comparisons of mean kurtosis in the superior longitudinal fasciculus, forceps major, and forceps minor are shown in the top row (A-C). Within older adults, associations between age and MK in these white matter tracts are shown in the bottom row (D-F). Significant correlations were seen between MK and age in each white matter tract ( $P_s < 10^{-3}$ ).

2 Group (younger, older)  $\times$  6 (subcortical grey matter) Region ANOVA. A significant interaction between Group and Region was observed ( $P < 10^{-3}$ ;  $F = 28.004$ ). *Post hoc* *t*-tests revealed that the older adult group had higher mean  $R_2^*$  than the younger group in the putamen ( $P < 10^{-3}$ ), globus pallidus ( $P < 10^{-3}$ ), caudate nucleus ( $P < 10^{-3}$ ), dentate nucleus ( $P < 10^{-3}$ ), and hippocampus ( $P < 10^{-3}$ ), but not in the thalamus ( $P = 0.242$ ). These comparisons are shown in **Figure 2** and are summarized in **Table 2**.

### 3.4 Effects of age on $R_2^*$ within older adults

Older age was correlated with lower  $R_2^*$  in the caudate nucleus ( $r = -0.268$ ;  $P = 0.011$ ). No significant correlations between age and  $R_2^*$  were observed in the putamen ( $r = 0.046$ ;  $P = 0.666$ ), globus pallidus ( $r = 0.065$ ;  $P = 0.545$ ), dentate nucleus ( $r = -0.065$ ;  $P = 0.544$ ), thalamus ( $r = -0.155$ ;  $P = 0.143$ ), or hippocampus ( $r = -0.148$ ;  $P = 0.164$ ).

### 3.4 Effects of age on $R_2^*$ within older adults

In the older adult group, MK and  $R_2^*$  were significantly positively associated in all grey matter ROIs, including the putamen ( $r = 0.691$ ;  $P < 10^{-3}$ ), globus pallidus ( $r = 0.511$ ;  $P < 10^{-3}$ ), caudate nucleus ( $r = 0.592$ ;  $P < 10^{-3}$ ), dentate nucleus ( $r = 0.698$ ;  $P < 10^{-3}$ ), thalamus ( $r = 0.340$ ;  $P = 0.001$ ), and hippocampus ( $r = 0.260$ ;  $P = 0.014$ ). The MK- $R_2^*$  correlations in the older adult group remained significant after controlling for age ( $P_s < 0.026$ ). In the younger group, significant positive correlations were seen between MK and  $R_2^*$  in the putamen ( $r = 0.369$ ;  $P = 0.007$ ), globus pallidus ( $r = 0.692$ ;  $P < 10^{-3}$ ), caudate nucleus ( $r = 0.288$ ;  $P = 0.037$ ), dentate nucleus ( $r = 0.628$ ;  $P < 10^{-3}$ ), and hippocampus ( $r = 0.324$ ;  $P = 0.018$ ), but not in the thalamus ( $P = 0.110$ ). These associations are plotted in **Figure 4**.

### 3.5 Phantom experiments

The  $b = 0$  image and corresponding MK map for the agarose phantom with 4 vials containing different

concentrations of ferric citrate and agar without ferric citrate are shown in **Figure 5**. The ANOVA revealed a significant main effect of iron concentration ( $F = 247.96$ ,  $P < 10^{-3}$ ) and *post hoc* pairwise *t*-tests revealed significant differences in MK between all vials ( $P_s < 10^{-3}$ ). Mean MK in agar without ferric citrate was  $0.59 \pm 0.01$ . MK was found to increase as ferric citrate concentration increased with mean MK values of  $0.62 \pm 0.017$ ,  $0.67 \pm 0.018$ ,  $0.73 \pm 0.032$ , and  $0.77 \pm 0.038$  in vials with 0.06 mMol, 0.09 mMol, 0.12 mMol, and 0.15 mMol, respectively (**Figure 5**).

## 4. Discussion

This study examined how age affects MK in subcortical grey matter structures and in three white matter tracts as well as assessed the relationship between MK and iron content in subcortical grey matter. We found that age differentially affects MK in white matter and subcortical grey matter structures with older adults experiencing lower white matter MK and higher MK of iron-rich subcortical grey matter structures. Further, MK was significantly correlated with age in white matter tracts with lower MK associated with higher age. In subcortical grey matter of older adults, MK was significantly correlated to tissue  $R_2^*$  in each ROI and structures with higher iron levels showed higher MK, on average. Finally, the phantom experiment found that MK

**Table 2.** Age group differences in tissue  $R_2^*$

	Younger	Older	<i>t</i>
Putamen	21.0 $\pm$ 1.4	30.5 $\pm$ 5.2	<b>187.0</b>
Globus pallidus	33.8 $\pm$ 3.4	38.9 $\pm$ 5.8	<b>36.30</b>
Caudate Nucleus	19.2 $\pm$ 1.5	22.3 $\pm$ 3.6	<b>38.98</b>
Dentate Nucleus	24.4 $\pm$ 2.7	27.8 $\pm$ 4.4	<b>29.11</b>
Thalamus	20.2 $\pm$ 1.2	19.9 $\pm$ 1.7	1.382
Hippocampus	15.9 $\pm$ 1.9	17.9 $\pm$ 1.8	<b>55.22</b>

*Notes.*  $R_2^*$  values in subcortical grey matter regions of interest. Data is presented as mean  $\pm$  standard deviation and units are  $s^{-1}$ . *Post hoc t*-tests were used for group comparisons of  $R_2^*$  in each ROI from which the *t*-statistics are shown.

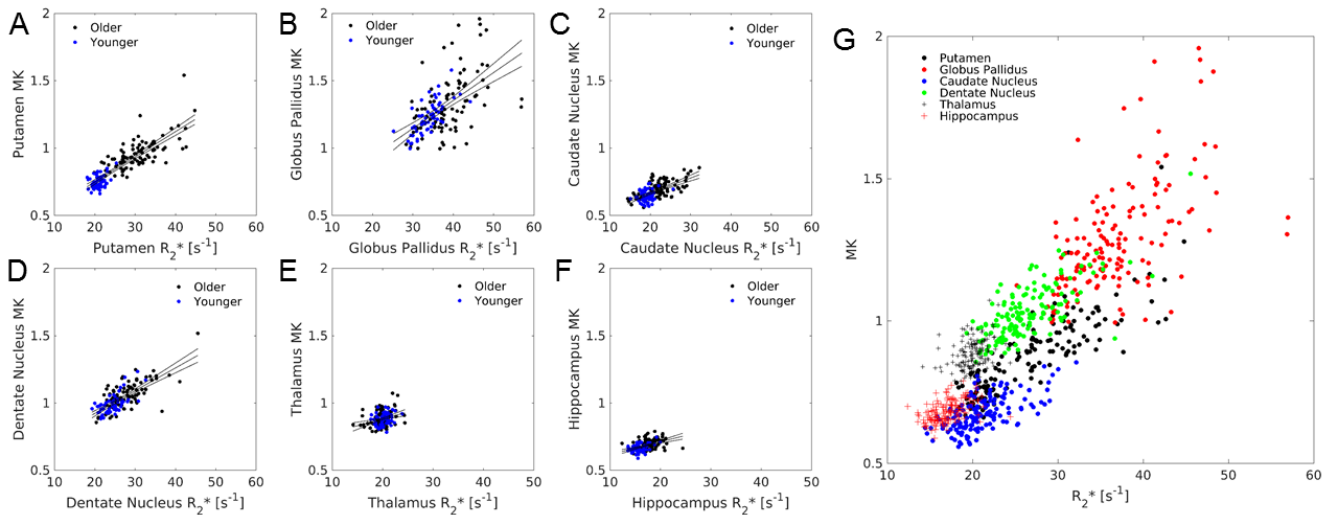


**Figure 4.** Correlations between MK and  $R_2^*$  in the putamen (A), globus pallidus (B), caudate nucleus (C), dentate nucleus (D), thalamus (E), and hippocampus (F). The association between MK and  $R_2^*$  in all subcortical ROIs is shown in G.

increases as iron concentration is increased.

Postmortem studies in humans have found age-related reductions in white matter volume and fibers in older adults<sup>16,17</sup>. These reductions should remove barriers to diffusion and manifest as decreased MK<sup>8,18</sup>. In agreement with this, we observed older adults had, on average, lower MK in white matter tracts as compared to the younger adult group. Other imaging studies using the DKI to examine age-related changes within white matter tracts found negative correlations between MK and age<sup>10-14</sup> and our correlations between MK and age in the older adult group replicate these findings.

We observed age-related increases in MK of all subcortical grey matter nuclei except the thalamus. Few studies have applied the kurtosis model to examine how aging affects subcortical grey matter. An earlier imaging study examining age-related changes MK in subcortical grey matter nuclei found changes depend on the nuclei under consideration with age is positively correlated with MK in the putamen and but negative correlations between age and MK in the caudate nucleus, globus pallidus, and thalamus<sup>11</sup>. Our results are in partial agreement with this study since we observed negative correlations between age and MK in the caudate nucleus and thalamus but no relationship was seen in the putamen or globus pallidus.

Histological and imaging studies have found that iron accrues in subcortical grey matter nuclei throughout life<sup>21-25</sup>. Consistent with these results, iron-sensitive MRI metrics were found to be elevated in older adults for all grey matter nuclei except for the thalamus ROI. Iron deposition has been found to alter DTI metrics from a single-tensor model (mean diffusivity, fractional anisotropy) within iron-rich grey matter nuclei in aging and disease<sup>26-28</sup> and this association may be due to the interaction between diffusion encoding

gradients with the magnetic fields generated by iron deposits<sup>29,30</sup>. Interestingly, MK was found to be correlated with iron in all subcortical grey matter nuclei in the older adult group. In the younger adult group, MK was correlated with iron in all grey matter structures except the thalamus.

We found MK in white matter was found to have values similar to values seen iron-rich subcortical grey matter nuclei. The similarity of these values may be due to the fact that these nuclei are permeated by small white matter bundles<sup>38-40</sup> and this observation agrees with an earlier study<sup>38</sup>. In both younger and older cohorts, structures with higher tissue  $R_2^*$  had, on average, higher MK. Consistent with this result, the phantom experiment found that MK increased as iron concentration increased. In subcortical grey matter, iron is primarily stored in ferritin. Together, ferritin and the white matter bundles may increase barriers to diffusion and lead to higher kurtosis values. Alternatively, iron content in subcortical grey matter nuclei will increase tissue  $R_2$  or  $R_2^*$  and reduce the signal-to-noise ratio. This reduction in signal-to-noise ratio may increase MK<sup>41,42</sup>.

The results presented here suggest iron content alters MK by adding additional barriers to diffusion or by reducing the signal-to-noise ratio. The dependence of MK on iron may be problematic in interpreting MK changes in neurological conditions where iron is deposited. For example, in Parkinson's disease, iron deposition occurs alongside neuronal loss in the basal ganglia<sup>43-46</sup> and studies have found MK is increased in the basal ganglia of populations with Parkinson's disease<sup>19,20</sup>. The mechanism for these increases is unknown<sup>19</sup> since higher kurtosis values are thought indicate more complex tissue microstructure<sup>8,18</sup>. Given the relationship between iron and MK presented here, the increases in MK may be caused by iron deposition. However, additional studies are needed to confirm that the relationship holds in a pathologic population.



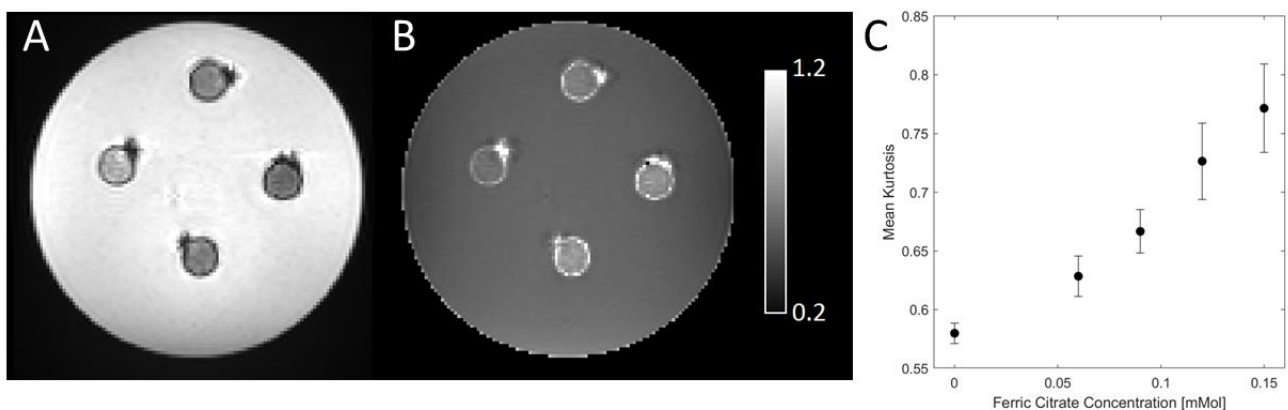


**Figure 5.** The  $b=0$  image is shown in A, mean kurtosis image is shown in B, and the relationship between ferric citrate concentration and mean kurtosis is shown in C.

This study is not without caveats. This study examined MK in iron-rich subcortical grey matter nuclei in older adults. Older adults tend to have elevated iron levels as compared to younger adults<sup>21-25</sup> and this iron deposition will increase tissue  $R_2$ , thereby reducing the signal-to-noise ratio. One limitation in the calculation of MK is signal-to-noise ratio and low signal-to-noise ratio may positively bias MK<sup>41</sup>. Here, we employed a denoising strategy to increase signal-to-noise ratios<sup>33</sup> and mitigate the positive bias on MK. However, we cannot rule out that noise biased MK values in the subcortical grey matter ROIs.

We observed age-related increases in MK and  $R_2^*$  in iron-rich grey matter structures, but age-related reductions in MK in white matter. Significant correlations were seen between MK and  $R_2^*$  in iron-rich grey matter structures and MK increased with iron concentration in a phantom. These findings indicate that higher MK may be related to iron content in iron-rich grey matter structures.

### Acknowledgements

This work was supported by R21-AG080282 and R01-AG072607 from the National Institutes of Health/ National Institute on Aging

### References

- Behler, A., Kassubek, J. & Muller, H.P. Age-Related Alterations in DTI Metrics in the Human Brain-Consequences for Age Correction. *Front Aging Neurosci* **13**, 682109 (2021).
- Bender, A.R., Volkle, M.C. & Raz, N. Differential aging of cerebral white matter in middle-aged and older adults: A seven-year follow-up. *Neuroimage* **125**, 74-83 (2016).
- Bennett, I.J., Madden, D.J., Vaidya, C.J., Howard, D.V. & Howard, J.H., Jr. Age-related differences in multiple measures of white matter integrity: A diffusion tensor imaging study of healthy aging. *Hum Brain Mapp* **31**, 378-390 (2010).
- Schwarz, S.T., *et al.* Diffusion tensor imaging of nigral degeneration in Parkinson's disease: A region-of-interest and

voxel-based study at 3 T and systematic review with meta-analysis. *Neuroimage Clin* **3**, 481-488 (2013).

- Zhang, Y., *et al.* Diffusion tensor imaging of the nigrostriatal fibers in Parkinson's disease. *Mov Disord* **30**, 1229-1236 (2015).
- Langley, J., *et al.* Diffusion tensor imaging of the substantia nigra in Parkinson's disease revisited. *Hum Brain Mapp* **37**, 2547-2556 (2016).
- Jensen, J.H., Helpert, J.A., Ramani, A., Lu, H. & Kaczynski, K. Diffusional kurtosis imaging: the quantification of non-gaussian water diffusion by means of magnetic resonance imaging. *Magn Reson Med* **53**, 1432-1440 (2005).
- Szczepankiewicz, F., *et al.* The link between diffusion MRI and tumor heterogeneity: Mapping cell eccentricity and density by diffusional variance decomposition (DIVIDE). *Neuroimage* **142**, 522-532 (2016).
- Cheung, M.M., *et al.* Does diffusion kurtosis imaging lead to better neural tissue characterization? A rodent brain maturation study. *Neuroimage* **45**, 386-392 (2009).
- Das, S.K., Wang, J.L., Bing, L., Bhetuwal, A. & Yang, H.F. Regional Values of Diffusional Kurtosis Estimates in the Healthy Brain during Normal Aging. *Clin Neuroradiol* **27**, 283-298 (2017).
- Gong, N.J., Wong, C.S., Chan, C.C., Leung, L.M. & Chu, Y.C. Aging in deep gray matter and white matter revealed by diffusional kurtosis imaging. *Neurobiol Aging* **35**, 2203-2216 (2014).
- Latt, J., *et al.* Regional values of diffusional kurtosis estimates in the healthy brain. *J Magn Reson Imaging* **37**, 610-618 (2013).
- Coutu, J.P., Chen, J.J., Rosas, H.D. & Salat, D.H. Non-Gaussian water diffusion in aging white matter. *Neurobiol Aging* **35**, 1412-1421 (2014).
- Benitez, A., Jensen, J.H., Falangola, M.F., Nietert, P.J. & Helpert, J.A. Modeling white matter tract integrity in aging with diffusional kurtosis imaging. *Neurobiol Aging* **70**, 265-275 (2018).

15. Falangola, M.F., *et al.* Age-related non-Gaussian diffusion patterns in the prefrontal brain. *J Magn Reson Imaging* **28**, 1345-1350 (2008).
16. Tang, Y., Nyengaard, J.R., Pakkenberg, B. & Gundersen, H.J. Age-induced white matter changes in the human brain: a stereological investigation. *Neurobiol Aging* **18**, 609-615 (1997).
17. Marner, L., Nyengaard, J.R., Tang, Y. & Pakkenberg, B. Marked loss of myelinated nerve fibers in the human brain with age. *J Comp Neurol* **462**, 144-152 (2003).
18. Hui, E.S., Cheung, M.M., Qi, L. & Wu, E.X. Towards better MR characterization of neural tissues using directional diffusion kurtosis analysis. *Neuroimage* **42**, 122-134 (2008).
19. Wang, J.J., *et al.* Parkinson disease: diagnostic utility of diffusion kurtosis imaging. *Radiology* **261**, 210-217 (2011).
20. Welton, T., *et al.* Microstructure of Brain Nuclei in Early Parkinson's Disease: Longitudinal Diffusion Kurtosis Imaging. *J Parkinsons Dis* **13**, 233-242 (2023).
21. Hallgren, B. & Sourander, P. The effect of age on the non-haemin iron in the human brain. *J Neurochem* **3**, 41-51 (1958).
22. Aquino, D., *et al.* Age-related iron deposition in the basal ganglia: quantitative analysis in healthy subjects. *Radiology* **252**, 165-172 (2009).
23. Bilgic, B., Pfefferbaum, A., Rohlfing, T., Sullivan, E.V. & Adalsteinsson, E. MRI estimates of brain iron concentration in normal aging using quantitative susceptibility mapping. *Neuroimage* **59**, 2625-2635 (2012).
24. Haacke, E.M., *et al.* Correlation of putative iron content as represented by changes in R2\* and phase with age in deep gray matter of healthy adults. *J Magn Reson Imaging* **32**, 561-576 (2010).
25. Pfefferbaum, A., Adalsteinsson, E., Rohlfing, T. & Sullivan, E.V. MRI estimates of brain iron concentration in normal aging: comparison of field-dependent (FDRI) and phase (SWI) methods. *Neuroimage* **47**, 493-500 (2009).
26. Pfefferbaum, A., Adalsteinsson, E., Rohlfing, T. & Sullivan, E.V. Diffusion tensor imaging of deep gray matter brain structures: effects of age and iron concentration. *Neurobiol Aging* **31**, 482-493 (2010).
27. Langley, J., Huddleston, D.E. & Hu, X. Nigral diffusivity, but not free water, correlates with iron content in Parkinson's disease. *Brain Commun* **3**, fcab251 (2021).
28. Langley, J., Hussain, S., Flores, J.J., Bennett, I.J. & Hu, X. Characterization of age-related microstructural changes in locus coeruleus and substantia nigra pars compacta. *Neurobiol Aging* **87**, 89-97 (2020).
29. Zhong, J., Kennan, R.P. & Gore, J.C. Effects of susceptibility variations on NMR measurements of diffusion. *J Magn Reson* **95**, 267-280 (1991).
30. Novikov, D.S., Reisert, M. & Kiselev, V.G. Effects of mesoscopic susceptibility and transverse relaxation on diffusion NMR. *J Magn Reson* **293**, 134-144 (2018).
31. Smith, S.M., *et al.* Advances in functional and structural MR image analysis and implementation as FSL. *NeuroImage* **23 Suppl 1**, S208-219 (2004).
32. Woolrich, M.W., *et al.* Bayesian analysis of neuroimaging data in FSL. *NeuroImage* **45**, S173-186 (2009).
33. Veraart, J., *et al.* Denoising of diffusion MRI using random matrix theory. *Neuroimage* **142**, 394-406 (2016).
34. Andersson, J.L., Skare, S. & Ashburner, J. How to correct susceptibility distortions in spin-echo echo-planar images: application to diffusion tensor imaging. *NeuroImage* **20**, 870-888 (2003).
35. Smith, S.M. Fast robust automated brain extraction. *Hum Brain Mapp* **17**, 143-155 (2002).
36. Henriques, R.N., *et al.* Diffusional Kurtosis Imaging in the Diffusion Imaging in Python Project. *Front Hum Neurosci* **15**, 675433 (2021).
37. He, N., *et al.* Improved Neuroimaging Atlas of the Dentate Nucleus. *Cerebellum* **16**, 951-956 (2017).
38. Maiter, A., *et al.* Investigating the relationship between diffusion kurtosis tensor imaging (DKTI) and histology within the normal human brain. *Sci Rep* **11**, 8857 (2021).
39. Percheron, G., Yelnik, J. & Francois, C. A Golgi analysis of the primate globus pallidus. III. Spatial organization of the striato-pallidal complex. *J Comp Neurol* **227**, 214-227 (1984).
40. Yelnik, J., Francois, C., Percheron, G. & Heyner, S. Golgi study of the primate substantia nigra. I. Quantitative morphology and typology of nigral neurons. *J Comp Neurol* **265**, 455-472 (1987).
41. Glenn, G.R., Tabesh, A. & Jensen, J.H. A simple noise correction scheme for diffusional kurtosis imaging. *Magn Reson Imaging* **33**, 124-133 (2015).
42. Jensen, J.H. & Helpert, J.A. MRI quantification of non-Gaussian water diffusion by kurtosis analysis. *NMR Biomed* **23**, 698-710 (2010).
43. Dexter, D.T., *et al.* Increased nigral iron content in postmortem parkinsonian brain. *Lancet* **2**, 1219-1220 (1987).
44. Langley, J., *et al.* Reproducible detection of nigral iron deposition in 2 Parkinson's disease cohorts. *Mov Disord* **34**, 416-419 (2019).
45. Du, G., *et al.* Combined R2\* and diffusion tensor imaging changes in the substantia nigra in Parkinson's disease. *Mov Disord* **26**, 1627-1632 (2011).
46. He, N., *et al.* Region-specific disturbed iron distribution in early idiopathic Parkinson's disease measured by quantitative susceptibility mapping. *Hum Brain Mapp* **36**, 4407-4420 (2015).